ACS APPLIED MATERIALS & INTERFACES

Research Article

www.acsami.org

SiO_2@YBO_3:Eu^{3+} Hollow Mesoporous Spheres for Drug Delivery Vehicle

Guixin Yang, Shili Gai,*[,†] Fengyu Qu,[‡] and Piaoping Yang*[,†]

[†]Key Laboratory of Superlight Materials and Surface Technology, Ministry of Education, Harbin Engineering University, Harbin 150001, P. R. China

[‡]Key Laboratory of Semiconductor Nanocomposite Materials, Ministry of Education, Harbin Normal University, Harbin, 150025, P. R. China

ABSTRACT: A novel bifunctional (fluorescent, mesoporous) hollow sphere was prepared by coating luminescent YBO_3:Eu^{3+} nanoparticles onto uniform hollow mesoporous silica spheres (HMSs), derived from an etching strategy using spherical Fe_3O_4 as templates. The composites exhibit typical mesoporous shells, large interior space, high surface area, and well dispersed nanospheres with controlled size. In addition, the textural properties including the specific surface and pore volume can be easily altered by simply tuning of the spherical Fe_3O_4 cores. Upon ultraviolet (UV) excitation, the composite shows the characteristic $^5D_0$−$^7F_{1-4}$ red emission lines of Eu^{3+} even after loading of the model drug. The composite with a large surface area and cavity was used as the host for loading the anticancer drug doxorubicin hydrochloride (DOX). It is observed that the multifunctional composites exhibit an obvious sustained release property and released in texture- and pH-sensitive patterns. Particularly, the down-conversion (DC) fluorescence intensity of the bifunctional vehicle increases with the release of drug molecules, making it possible to track the position and the drug release amount of the drug carrier system and to detect them by the change of fluorescence intensity.

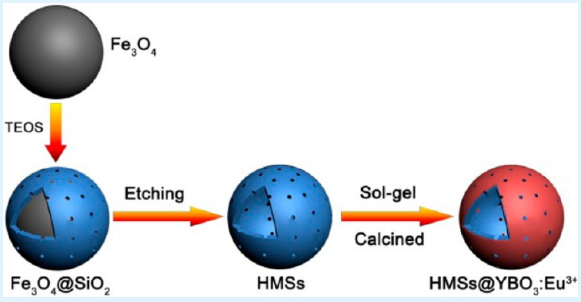

KEYWORDS: *YBO_3:Eu^{3+}, silica, hollow, drug release, luminescence, mesoporous*

INTRODUCTION

Over the past decade, many efforts have been devoted to design novel sustained/controlled drug delivery systems, which are superior to commercial administrated drugs in terms of dosage, due to their high delivery efficiency, low side-effects, and low toxicity.[1−6] To date, various polymer,[7−12] inorganic,[13−19] and inorganic/organic hybrid materials[20−24] with diverse structures and shapes have been employed as vehicles for drug delivery. Particularly, mesoporous silica based materials have gained considerable attention in the delivery of different drugs due to their excellent biocompatibility, biodegradability, tailored mesoporous structure, high surface area, and facile surface modification.[25−31] More importantly, by combining or grafting functional groups, such as magnetic nanocrystals,[32−37] Au particles,[38−43] quantum dots,[44−48] tumor-targeting moieties[49,50] and PEG[51−55] onto the mesoporous silica surface, multifunctional silica-based composites have been produced in the forms of core−shell, embedded, and rattle-type structures, which exhibit rapid growth in the applications of bioimaging diagnosis, drug delivery, and therapy.

Notably, fluorescence functionalized mesoporous silica drug delivery vehicle can be fabricated by the combination of mesoporous silica structure with fluorescent materials, and have attracted special interest because of their photoluminescence. However, as the commonly used fluorescent components, organic dyes usually suffer from rapid photobleaching, poor stability and low quantum yield,[56] and quantum dots (QDs) are optical blinking and toxicity,[57] making both of them unsuitable for applications in biomedicine.[58,59] For comparison, rare earth (RE) based inorganic materials exhibit good luminescent properties, chemical/photochemical inertness, and low toxicity,[60−67] which seem to be excellent candidates for organic dyes and quantum dots. Our group first exploited RE-doped nanophosphors for drug delivery, and core−shell structured functional composites have been reported.[68,69] However, the relatively low surface area and small pore volume may limit their application. Thus, developing a kind of functional hollow mesoporous silica spheres should be highly potential, not only due to their silica characteristics but for their large interior space and tunable porous shell, which is suitable for loading more drugs and diffusing the drug molecules through the channels freely. Moreover, different from the extensive reports on magnetism functionalized hollow silica spheres for application as drug carriers,[70−75] fluorescence, especially RE based phosphors, functionalized hollow silic spheres have been comparatively much less reported.

In general, most hollow silica spheres have been synthesized by templating strategies that involve the preparation of an inner core

Received: April 12, 2013
Accepted: May 24, 2013
Published: May 24, 2013

   dx.doi.org/10.1021/am401349z | *ACS Appl. Mater. Interfaces* 2013, 5, 5788−5796

and a layer of outer shell and subsequent removal of the core template. In principle, the inner core is completely different from the outer shell, which makes it possible to selectively remove the cores by chemical etching or calcination. Magnetic particles, especially Fe_3O_4, are chemically stable and easily obtained with spherical shape and tunable sizes, which are suitable as core templates. A selective etching process to remove the Fe_3O_4 core part of as-prepared core−shell-structured Fe_3O_4@SiO_2 is an effective method to prepare hollow silica spheres.[31,74] $REBO_3$ (RE = La−Lu, Y) gained plentiful attention because of their outstanding properties.[76−79] Particularly, YBO_3:Eu red phosphors have become a research focus due to its vacuum ultraviolet transparency, high optical efficiency, low toxicity, and exceptional fluorescent damage threshold.[80−82] Compared with the conventional organic dyes and quantum dots, it avoids the shortcomings of quenching and chronic toxicities *in vivo*, thus making it possible to apply as a fluorescent label for tracking and detecting the drug release in disease therapy.

In this study, we developed a straightforward route to produce SiO_2 capsule coated YBO_3:Eu^{3+} (SiO_2@YBO_3:Eu^{3+}) hollow composites with large hollow interiors using Fe_3O_4 nanospheres as a sacrificial template. The sizes of Fe_3O_4 cores were altered to tune the size and textural properties of the functional systems. And doxorubicin hydrochloride (DOX) was picked as a model drug to illustrate the release properties of this functional composite. While DOX was introduced into the systems, and the drug release behavior was examined. In addition, the MTT assay was performed to evaluate the short-term cytotoxicity of the functional carrier.

EXPERIMENTAL SECTION

Chemicals and Materials. Ethylene glycol (EG), $FeCl_3·6H_2O$, ammonia (25−28%), sodium acetate (CH_3COONa), ethylenediamine (ETH), tetraethoxysilane (TEOS), cetyltrimethylammonium bromide (CTAB), H_3BO_3, polyethylene glycol (PEG, M_w = 10 000 g mol^{-1}), trisodium citrate, ethylene glycol, hydrochloric acid (A. R.), $Y(NO_3)_3·6H_2O$ (≥99.0%, A. R.), and Eu_2O_3 (99.99%) were all purchased from Sinopharm Chemical Reagent Co., Ltd. (China). All of the chemical reagents in the experiment were used as received. $Eu(NO_3)_3$ and $Y(NO_3)_3$ were prepared by dissolving stoichiometric amounts of Eu_2O_3 and Y_2O_3 in nitric acid, respectively. Then the superfluous acid and water were evaporated.

Synthesis. *Synthesis of Fe_3O_4 Template Spheres.* Fe_3O_4 with a particle size of about 90 nm was synthesized using a typical procedure as follows: 1.0 g of $FeCl_3·6H_2O$ and 3.0 g of sodium acetate were dissolved in 30 mL of EG/ETH [EG/ETH = 2:1 (v/v)] by vigorously stirring. Then the mixture was transferred into an autoclave and heated at 200 °C for 24 h. After cooling to room temperature, the resulting black precipitate was washed repeatedly with ethanol and deionized water and dried in the air. The final sample was denoted as Fe_3O_4-A.

As for the synthesis of Fe_3O_4 with a particle size of 180 nm, 3.25 g of $FeCl_3·6H_2O$, 1.3 g of trisodium citrate, and 6.0 g of CH_3COONa were added in 100 mL of EG under constant stirring. The as-obtained solution was transferred into a 200 mL autoclave and maintained at 200 °C for 10 h. The final-product was washed with deionized water and ethanol several times and dried at 80 °C, which was designated as Fe_3O_4-B. Fe_3O_4 has a mean diameter of 300 nm and was synthesized according to our previous article.[69] The obtained product was designated as Fe_3O_4-C.

Preparation of Hollow Mesoporous SiO_2 Spheres (HMSs). First, synthesis of the core−shell Fe_3O_4@SiO_2 structure was carried out following the modified Stöber sol−gel process: 100 mg of Fe_3O_4 particles with a mean size of 90 nm were treated with 0.1 M HCl by ultrasonication for 30 min. After separation by centrifugation, the Fe_3O_4 sample was well dispersed in a solution containing ethanol (80 mL), CTAB (0.15 g), deionized water (20 mL), and aqueous ammonia (1 mL). Then 0.065 mL of TEOS was introduced dropwise to the reaction mixture under mechanical stirring for 12 h at ambient temperature to give rise to Fe_3O_4@SiO_2. Second, Fe_3O_4@SiO_2 nanoparticles were treated with concentrated HCl (37%) in a water bath at 60 °C and then isolated by centrifugation. The obtained white particles were dried in the air at 60 °C for 12 h, which was designed as HMSs-A. HMSs-B and HMSs-C were fabricated by a similar process.

Synthesis of HMSs@YBO_3:Eu^{3+} Composites. A total of 0.6894 g of $Y(NO_3)_3·6H_2O$, 0.4 mL of $Eu(NO_3)_3$ (0.5 M), 0.185 g of H_3BO_3 compound, and 0.5 mL of glycerol were added to the water/ethanol [1:6 (v/v)] solution until dissolution. Then 4 g of PEG-10000 was introduced to the mixed solution with stirring for around 2 h, followed by the addition of HMSs-A. Continuously stirred for 48 h, the particles were collected by centrifugation and dried at 100 °C quickly. Finally, the dried sample was heated to 800 °C with a heating rate of 2 °C/min and kept at this temperature for 2 h to form the final composite, which was designed as HMMs-A@YBO_3:Eu^{3+}. HMMs-B@YBO_3:Eu^{3+} and HMMs-C@YBO_3:Eu^{3+} were prepared through a similar procedure

DOX Release Test. In a typical process for the loading of DOX on HMSs@YBO_3:Eu^{3+}, 30 mg of HMSs@YBO_3:Eu^{3+} capsules were mixed with 2.5 mg of DOX dispersed in PBS solution (5 mL). The system was protected from light, stirred for 24 h, and washed with PBS solution, yielding the DOX loaded particles (DOX−HMSs@YBO_3:Eu^{3+}). The amount of DOX stored in the samples was measured by UV−vis spectrophotometer at 480 nm. And the loading efficiency (LE%) was determined as follows: LE % = $(M_{DOX1} - M_{DOX2})/M_{DOX1} \times 100\%$, where M_{DOX1} is the original DOX amount and M_{DOX2} is the unloaded DOX amount.

The release test was performed by immersing a DOX−HMSs@YBO_3:Eu^{3+} sample in 10 mL of PBS under gentle stirring under dark conditions, and the immersing temperature was kept at 37 °C. At a given time, PBS solution was taken and immediately replaced with an equal volume of fresh PBS.

Short-Term Cytotoxicity Assay. The short-term cytotoxicity of the composite was assessed by the standard 3-(4,5-dimethylthiazol-2-yl)-2,5-diphenyltetrazolium bromide (MTT) assay.[83,84] Typically, L929 fibroblast cells were cultured in 5% CO_2 at 37 °C in 200 μL of fresh culture media for 24 h. The HMSs-B@YBO_3:Eu^{3+} sample was sterilized by UV irradiation then diluted at concentrations of 6.25, 12.5, 25, 50, 100, and 200 μg/mL in growth media to replace the original one and incubate cells continuously under the same conditions. After that, 5 mg/mL of MTT in PBS was added and incubated with the cells for another 4 h. Finally, dimethyl sulfoxide (DMSO) was added and transferred to a shaking table. The absorbance of the suspension was monitored with a microplate reader at 570 nm.

Characterization. The powder X-ray diffraction (XRD) measurements were acquired with a Rigaku TTR III diffractometer by using graphite monochromatic Cu Kα radiation (λ = 0.15405 nm). And the scanning rate is 10°/min in a 2θ range of 10°−80°. The size and morphology of the samples were studied on a scanning electron microscope (SEM, S-4800, Hitachi) equipped with an energy dispersive X-ray spectrum (EDS, JEOL

JXA-840). Transmission electron microscopy (TEM) and high-resolution transmission electron microscopy (HRTEM) images were taken on a FEI Tecnai G^2 S-Twin electron microscope operating at 200 kV. The X-ray photoelectron spectra (XPS) were measured on an ECSALAB 250. The observed binding energies were corrected by referring to the C 1s peak of contaminating carbon at 285.0 eV. An N_2 adsorption measurement was performed on a Micromeritics ASAP 2010 analyzer at liquid nitrogen temperature (77 K). The specific surface area was obtained from the Brunauer–Emmett–Teller (BET) method, and pore size distribution was calculated from the adsorption branch of the isotherm. FT-IR spectra were measured on an AVATAR 360 FT-IR spectrophotometer using a standard KBr pellet technique. The absorbance of DOX was obtained on a TU-1901 UV/vis spectrophotometer. The photoluminescence (PL) measurements were investigated using a Hitachi F-7000 spectrophotometer equipped with a 150 W xenon lamp as the excitation source.

RESULTS AND DISCUSSION

The synthetic procedure for the preparation of HMSs@YBO_3:Eu^{3+} is illustrated in Scheme 1. First, a silica monolayer

Scheme 1. Schematic Illustration of the Synthetic Procedure for HMSs@YBO_3:Eu^{3+} Composite

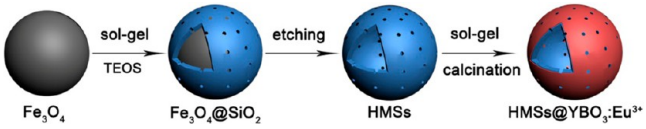

is coated onto the as-prepared magnetic Fe_3O_4 particles using the Stöber sol–gel procedure to realize a core–shell structured Fe_3O_4@silica composite. Subsequently, the Fe_3O_4 templates were etched by 0.1 M HCl yielding the uniform silica hollow spheres with a mesoporous shell. And YBO_3:Eu^{3+} phosphors were coated onto the hollow silica layer *via* a modified sol–gel process to form the final bifunctional (luminescent and porous) composite, which was denoted as HMSs@YBO_3:Eu^{3+}.

Figure 1 offers the XRD patterns of Fe_3O_4 (180 nm), HMSs, and HMSs-B@YBO_3:Eu^{3+}. For Fe_3O_4 nanoparticles, all the peaks can be readily indexed to the standard data for Fe_3O_4 (JCPDS No. 19–0629). It is obvious that only the amorphous SiO_2 peak

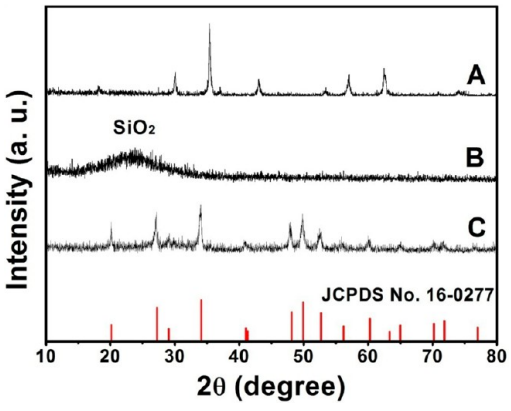

Figure 1. XRD patterns of Fe_3O_4-B prepared at 200 °C for 10 h (A), HMSs (B), and HMSs-B@YBO_3:Eu^{3+}(C). The vertical bars show the peak positions and intensities for pure YBO_3 (JCPDS 16-0277) as a reference.

can be detected in Figure 1B, showing that the Fe_3O_4 cores have been completely removed. In the XRD pattern of HMSs-B@YBO_3:Eu^{3+} (Figure 1C), the position and intensities of the main diffraction peaks match well with the standard YBO_3 (JCPDS No. 16-0277), revealing that YBO_3:Eu^{3+} phosphor has successfully been functionalized on the SiO_2 porous shell.

Well-defined Fe_3O_4 particles with tunable size were synthesized using a solvothermal method, and the respective SEM image is provided in Figure 2A1, B1, and C1. Clearly, the three kinds of Fe_3O_4 samples all consist of uniform spheres with a mean diameter of 90, 180, and 300 nm, respectively. In the etching process, the Fe_3O_4 cores can be removed away from the silica shell by hydrochloric acid at an elevated temperature, which implies that the silica shell has a hollow interior. This makes it possible to prepare HMSs with tunable particle sizes by using different sized Fe_3O_4 spheres as templates. As depicted in Figure 2, the size and morphology of the hollow nanospheres are mainly maintained. In addition, the selected broken spheres (pointed by the circles) in Figure 2A2, B2, C2 confirm the hollow structures of all the samples. As for YBO_3:Eu^{3+} functionalized hollow silica spheres (HMSs@YBO_3:Eu^{3+}), the size and spherical morphologies are still kept, indicating that introduction of YBO_3:Eu^{3+} is lacking any influence on the shape and size. What is more, the cavity of the hollow spheres can still be observed in Figure 2A3, B3, and C3, indicating the maintenance of the hollow structures.

The structure of the samples was further investigated by TEM images in Figure 3. We can see that well dispersed Fe_3O_4 spheres with different particle sizes are obtained (Figure 3A1, B1, and C1), corresponding well with the SEM images. It is apparent that the color of HMSs turns from black to gray after removal of the Fe_3O_4 cores, and the spherical shape and size of the SiO_2 capsules remain unchanged. The respective thin shell is determined to be about 10, 12, and 13 nm in thickness, as depicted in Figure 3A2, B2, and C2. The porous shell facilitates the sol (phosphors precursor) to diffuse in or out, resulting in the formation of HMSs@YBO_3:Eu^{3+} (Figure 3A3, B3, and C3). Additionally, the size and shape of all HMSs@YBO_3:Eu^{3+} products keeps in accordance with the SEM images (Figure 2). Careful observation reveals that the thicknesses of the samples' shells increase slightly in comparison with pure HMSs, which mainly comes from the deposited phosphors

Figure 4A represents a magnified TEM image of HMSs-B@YBO_3:Eu^{3+}, which clearly displays the inside hollow and outside shell structure of the sample. The distinct lattice fringes in the HRTEM image (Figure 4B) reveal that the sample has a high crystallinity feature, agreeing well with the XRD analysis. The determined interplanar distance of 0.30 nm is indexed to the (101) plane of hexagonal YBO_3 (JCPDS No. 16-0277). This is also supported by the FFT pattern (Figure 4C), which shows the diffraction spots of the (101) planes of YBO_3. In addition, the EDS (Figure 4D) demonstrates the existence of B, Si, O, and Y elements.

Figure 5 depicts the XPS spectra of HMSs-B@YBO_3:Eu^{3+}. All the binding energy of B (1s, 193.1 eV), Y ($3d_{5/2}$, 155.8 eV; $3d_{3/2}$, 158.0 eV), Si (2p, 102.7 eV), and O (1s, 531.7 eV) can be detected. Banding the XRD and EDS results together, it is inferred that these signals can be ascribed to HMSs-B@YBO_3:Eu^{3+}. Due to the very low doping concentration (5 mol %), Eu^{3+} cannot be evidenced by XPS spectra.

N_2 adsorption experiment results of HMSs-B and HMSs-B@YBO_3:Eu^{3+} are given in Figure 6. From the isotherms (Figure 6, left), we can see that the two samples show characteristic IV isotherms with H_1-typed hysteresis loops associated with the

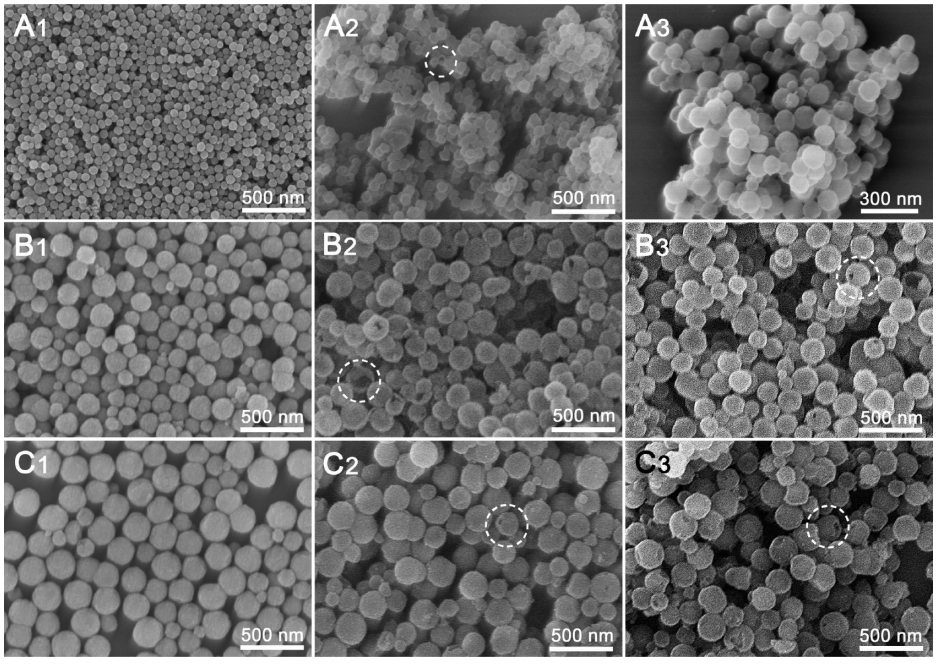

Figure 2. SEM images of Fe_3O_4-A (A1), HMSs-A (A2), HMSs-A@YBO_3:Eu^{3+} (A3); Fe_3O_4–B (B1), HMSs-B (B2), HMSs-B@YBO_3:Eu^{3+} (B3); Fe_3O_4-C (C1), HMSs-C (C2), HMSs-C@YBO_3:Eu^{3+} (C3).

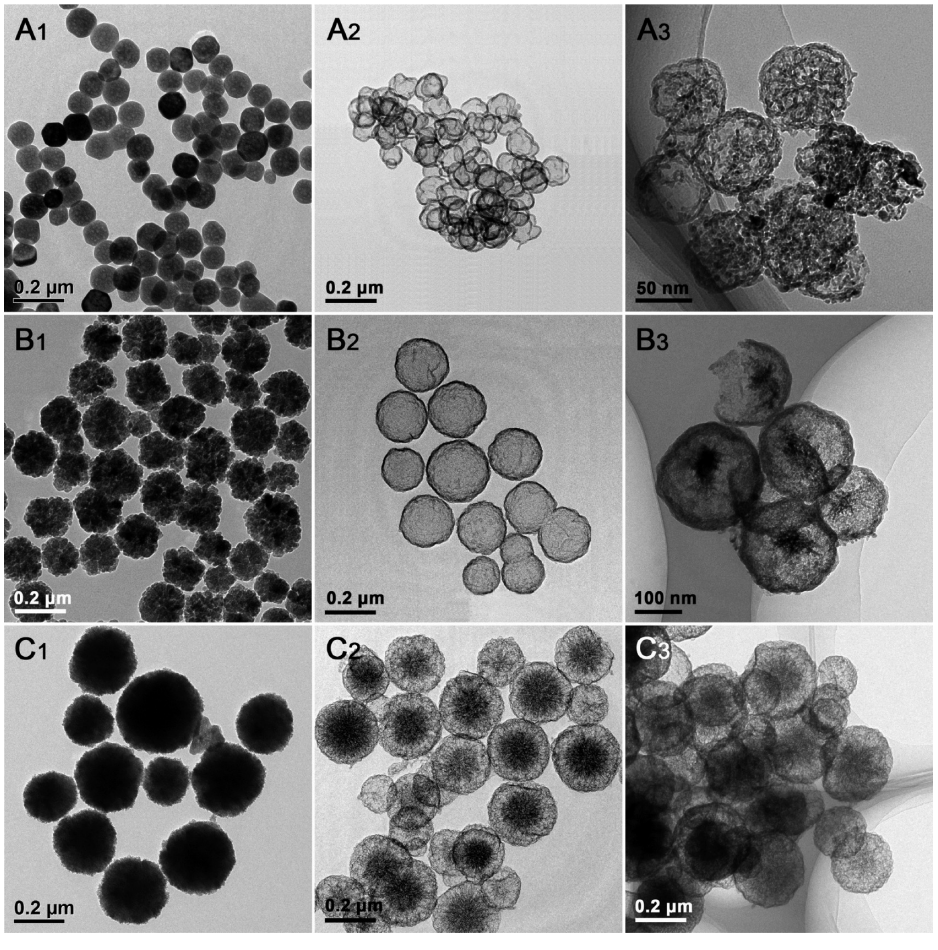

Figure 3. TEM images of Fe_3O_4-A (A1), HMSs-A (A2), HMSs-A@YBO_3:Eu^{3+} (A3); Fe_3O_4-B (B1), HMSs-B (B2), HMSs-B@YBO_3:Eu^{3+} (B3); Fe_3O_4-C (C1), HMSs-C (C2), HMSs-C@YBO_3:Eu^{3+} (C3).

mesoporous structure, indicating that the introduction of the YBO_3:Eu^{3+} phosphors onto the porous shell have not changed the mesoporous structure. The textural parameters of HMSs and HMSs@YBO_3:Eu^{3+} with different particle sizes (90, 180, and 300

dx.doi.org/10.1021/am401349z | ACS Appl. Mater. Interfaces 2013, 5, 5788−5796

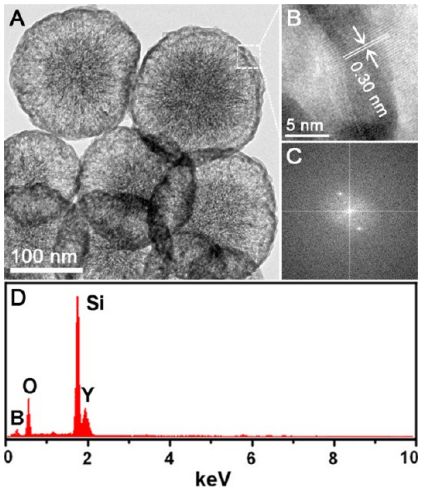

Figure 4. TEM image (A), HRTEM image (B), FFT pattern (C), and EDS of HMSs-B@YBO_3:Eu^{3+} sample (D).

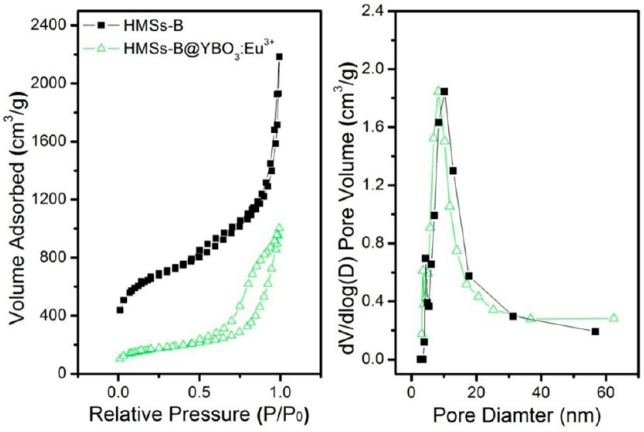

Figure 6. N_2 adsorption/desorption isotherm (left) and pore size distribution (right) of HMSs-B and HMSs-B@YBO_3:Eu^{3+}.

nm) are listed in Table 1. Obviously, all hollow silica spheres (HMSs) have high BET surface areas and BJH pore volume. Especially, the respective BET surface area and total pore volume of HMSs-B even reach 2311 m^2/g and 2.16 cm^3/g, which may originate from the mesoporous silica deriving from the removal of the CTAB template. As for the HMSs@YBO_3:Eu^{3+} samples, although the specific surface area, average pore size, and total pore volume are decreased compared with those of corresponding HMSs, the textural parameters are still highly superior enough realtive to the reported silica-based functional carriers,[68,69] suggesting its potential candidate in drug delivery. Moreover, the decrease of surface area, total pore volume, and

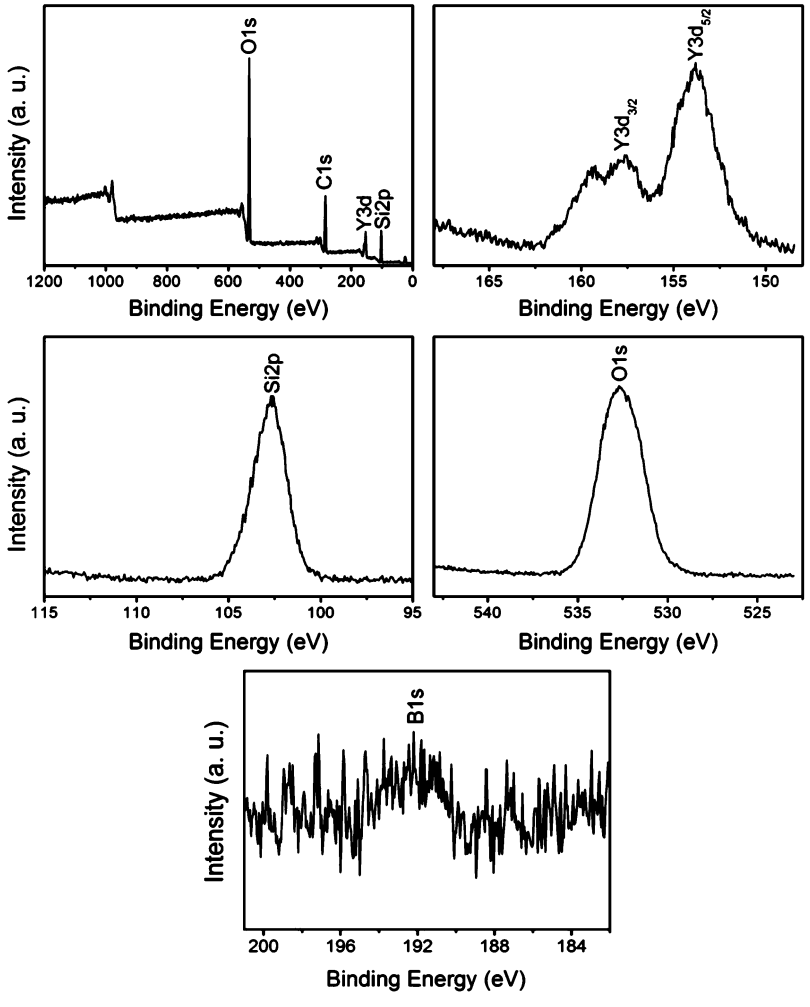

Figure 5. Survey and respective element XPS spectra of HMSs-B@YBO_3:Eu^{3+}.

Table 1. Textural Parameters of HMSs and HMSs@ $YBO_3:Eu^{3+}$

samples	S_{BET}[a] (m^2/g)	D (nm)	V_P (cm^3/g)
HMSs-A	347	10.42	0.66
HMSs-A@$YBO_3:Eu^{3+}$	96	6.53	0.27
HMSs-B	2311	10.31	2.16
HMSs-B@$YBO_3:Eu^{3+}$	506	8.31	0.98
HMSs-C	596	8.79	1.17
HMSs-C@$YBO_3:Eu^{3+}$	269	7.84	0.83

[a] S_{BET}, the BET specific surface area calculated in the relative pressure range from 0.05 to 0.2; D, the average diameter of mesopores calculated by the BJH method; V_p, the total pore volume calculated at a relative pressure of about 0.95.

average pore size also suggest that $YBO_3:Eu^{3+}$ nanocrystals were effectively integrated into the surface and channels of mesoporous silica shells.

Figure 7 shows the FT-IR spectra of pure DOX, HMSs-B@ $YBO_3:Eu^{3+}$, and HMSs-B@$YBO_3:Eu^{3+}$-DOX, respectively. In the

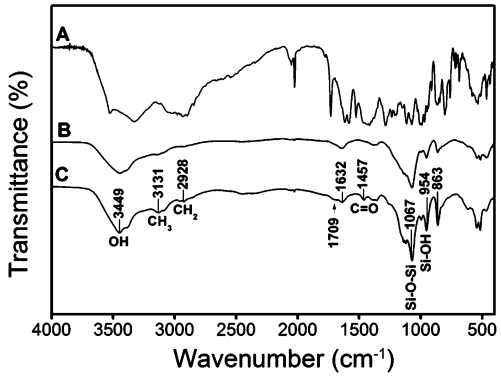

Figure 7. FT-IR spectra of pure DOX (A), HMSs-B@$YBO_3:Eu^{3+}$ (B), and HMSs-B@$YBO_3:Eu^{3+}$-DOX (C).

FT-IR spectrum of HMSs-B@$YBO_3:Eu^{3+}$ (Figure 7B), a broad peak at 3600−3200 cm^{-1} and a weak peak at 1632 cm^{-1} can be ascribed to the OH^- ions and O−H vibration of the H_2O molecule adsorbed on the surfaces. In addition, the characteristic vibrations of silica associated with Si−OH (954 cm^{-1}), Si−O−Si (1067 cm^{-1} and 863 cm^{-1}), and Si−O (471 cm^{-1}) are also apparent. As for the DOX loaded sample (Figure 7C), two small peaks at 3131 and 2928 cm^{-1} and some sharp peaks at 1709 and 1457 cm^{-1} can be observed. The former two bands should arise from $-CH_3$ and the asymmetric band of $-CH_2-$, while the latter two bands at 1709 and 1457 cm^{-1} can be attributed to the mode of the C═O stretching vibration in DOX molecules (Figure 7A). The above results give evidence for the existence of DOX on the surface of nanocomposites.

Figure 8 gives the excitation (left) and emission spectra (right) of HMSs-A@ $YBO_3:Eu^{3+}$, HMSs-B@$YBO_3:Eu^{3+}$, HMSs-C@ $YBO_3:Eu^{3+}$, and HMSs-B@YBO_3: Eu^{3+}-DOX. As a whole, all the HMSs@$YBO_3:Eu^{3+}$ samples exhibit much similar PL spectra except for a little change in the intensity. The excitation spectra (left) is composed of a broad $Eu^{3+}-O^{2-}$ charge transfer band (CTB) below 300 nm, and a series of weak transition lines in the range of 300−400 nm arising from f electrons of Eu^{3+}. According to the electronic transition from the 2p orbital of O^{2-} to the 4f orbital of Eu^{3+}, the CTB transition occurs. In the emission spectra (right) upon excitation at 230 nm, the characteristic $^5D_0-{}^7F_J$ (J = 1−4) emission peaks of Eu^{3+} are observed.[85−92] The $^5D_0-{}^7F_1$ peak at 594 nm is dominant, which is similar to other borate phosphors, and the two peaks at 613 and 628 nm both correspond to the $^5D_0-{}^7F_2$ transition. Notably, the PL emission is still obvious in the DOX loaded HMSs-B@$YBO_3:Eu^{3+}$ carrier (Figure 8D and inset), suggesting the potential to be tracked or detected during the drug release procedure.

To evaluate the capacity of HMSs@$YBO_3:Eu^{3+}$ for drug carriers, DOX was chosen as the model as a water-soluble anticancer drug to be loaded on HMSs@$YBO_3:Eu^{3+}$ capsules. In the loading process, the DOX molecules are stored in the hollow mesoporous spheres using an impregnation process. The respective loading amount is 131, 189, and 146 mg/g for HMSs-A@$YBO_3:Eu^{3+}$, HMSs-B@$YBO_3:Eu^{3+}$, and HMSs-C@ $YBO_3:Eu^{3+}$ from UV−vis spectra. Figure 9A gives the cumulative release curves of the loaded DOX from HMSs@$YBO_3:Eu^{3+}$-DOX composites in PBS buffer solutions at 37 °C and pH = 7.4. When HMSs@$YBO_3:Eu^{3+}$-DOX was immerged into PBS, a fast release was displayed in the initial 4 h, and then a sustained release property with a much slower release rate was observed. The fast release can be attributed to the adsorbed DOX on the outer surface of hollow spheres weakly, while the subsequent relatively slow release rate may be related with the slow diffusion of drug molecules from the inner surface. In addition, the strong electrostatic interaction between DOX molecules (positively charge) and the silica matrix (negatively charge) should also prevent the DOX molecules from the silica surface. Moreover, the difference of release rates for the three kinds of functional carriers should be related with their textural properties, such as specific surface area, mesporous pores, and pore volume. It should be noted that the functional system exhibits obvious pH-dependent properties (Figure 9B). A much faster release rate is found in acidic surroundings (pH = 4.0), because the enhanced positive potential of the silica surface weakens the electrostatic interaction with positively charged DOX, leading to a faster release. This intrinsic pH sensitive property is very important for a pH-triggered drug release, because the cancer tissue is acidic extracellularly under pathological conditions; the pH-sensitive carrier could be used to control the release of DOX, which is beneficial to reducing the toxic side effects for normal tissues.

Figure 10 shows the relationship between the luminescence intensity of HMSs-B@$YBO_3:Eu^{3+}$-DOX and the cumulative release amount of DOX (release time). It is found that that emission intensity of the functional carrier was strongly dependent on the released amount of DOX. It is apparent that the DC intensity is severely quenched by the loaded DOX and increases gradually with the continuous release of DOX, attaining its maximum when the release of the drug is complete. The organic groups with high-frequency phonon vibrations in the drug can quench the luminescence greatly.[56] The release of DOX may weaken the quenching effect, then enhance the luminescence intensity of drug carrier systems. The trend suggests the great potential of this kind of functional material to be tracked or monitored by the photoluminescence intensity during the release process.

A MTT assay was carried out to evaluate the short-term cytotoxicity of the HMSs-B@$YBO_3:Eu^{3+}$ sample. From Figure 11, we can see that the composite shows no obvious cytotoxicity against the L929 cells at a concentration of 6.25−200 μg/mL within 24 h. Even more than 95.3% cells remained alive when the concentration of sample reached 200 μg/mL. The results suggest a low short-term cytotoxicity of the system in all dosages, indicating the potential for biomedical use.

dx.doi.org/10.1021/am401349z | ACS Appl. Mater. Interfaces 2013, 5, 5788−5796

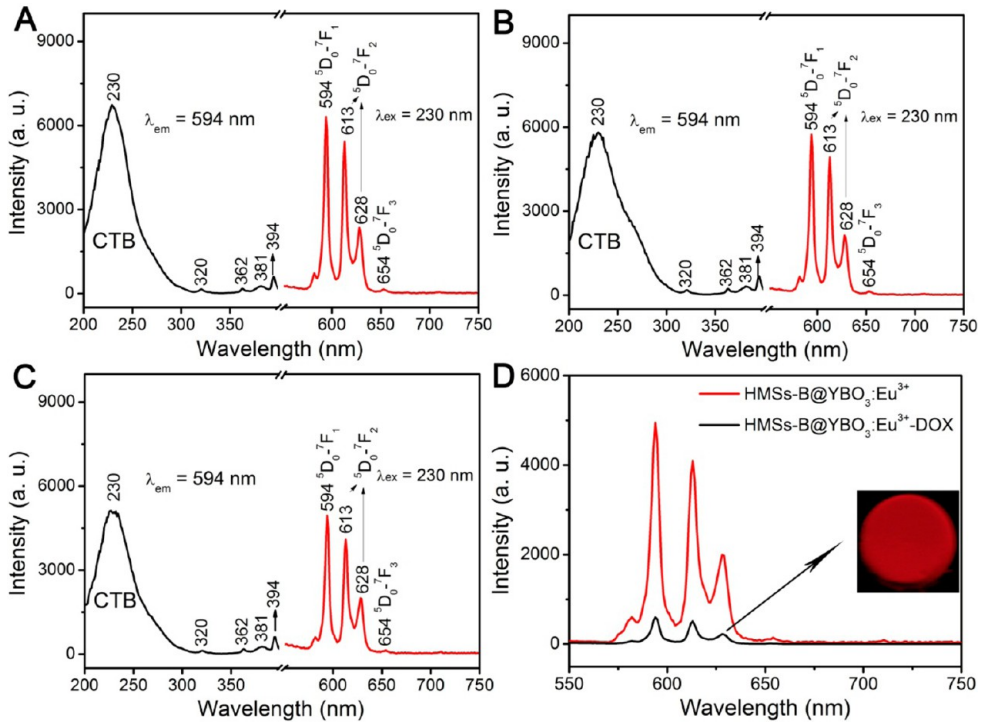

Figure 8. The excitation (left) and emission (right) spectra of HMSs-A@YBO_3:Eu^{3+} (A), HMSs-B@YBO_3:Eu^{3+} (B), HMSs-C@YBO_3:Eu^{3+} (C), and HMSs-B@ YBO_3:Eu^{3+}-DOX (D). The inset in D is the luminescent photograph of HMSs-B@ YBO_3:Eu^{3+}-DOX under 254 nm UV irradiation in the dark.

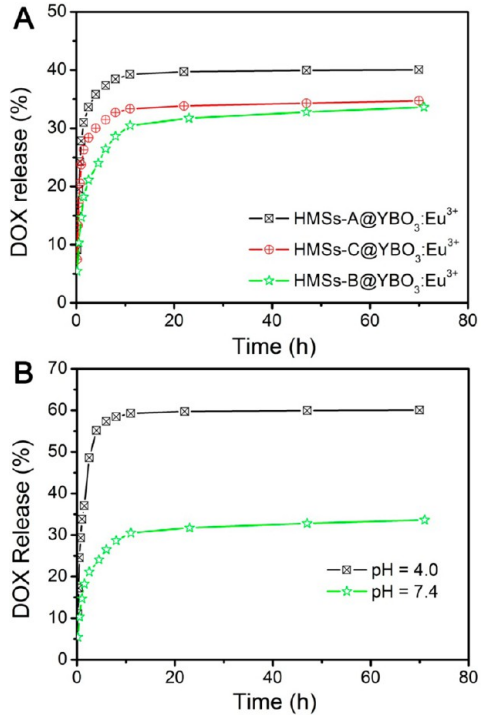

Figure 9. Cumulative DOX release from (A) HMSs-B@YBO_3:Eu^{3+}, HMSs-A@YBO_3: Eu^{3+}, and HMSs-C@YBO_3:Eu^{3+} samples in PBS buffer at pH = 7.4 as a function of the release time. (B) Cumulative DOX release from HMSs-B@YBO_3:Eu^{3+} at pH= 7.4 and pH = 4.0 PBS buffer.

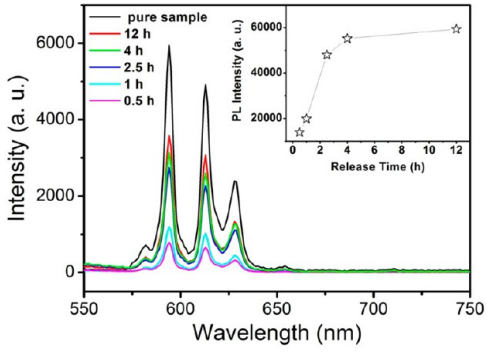

Figure 10. PL emission intensity of Eu^{3+} in HMSs-B@YBO_3:Eu^{3+}–DOX as a function of the release time.

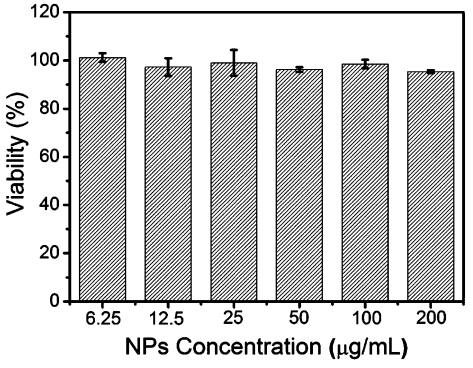

Figure 11. The L929 fibroblast cells' viability after incubating with HMSs-B@YBO_3:Eu^{3+} for 24 h and quantitative assays using the standard MTT method.

CONCLUSION

In summary, we have demonstrated a hard-templating procedure to prepare SiO_2@YBO_3:Eu^{3+} hollow nanospheres by selecting

dx.doi.org/10.1021/am401349z | ACS Appl. Mater. Interfaces 2013, 5, 5788−5796

different sized iron oxides as cores. This kind of bifunctional composite combines the advantages of hollow, mesoporous structure and luminescence, which are employed as drug carriers to study the loading and release efficiency using DOX as a model drug. This functional drug carrier exhibits obvious sustained properties and low short-term cytotoxicity. In particular, the luminescent intensity of drug loaded functional carriers increases with the release of DOX, making it possible to be monitored or tracked during the DOX release procedure. More importantly, the proposed strategy to obtain the functional hollow inorganic composites provides a feasible and efficient approach to fabricating other hollow or rattle-type structures to satisfy the needs of various applications.

AUTHOR INFORMATION

Corresponding Author

*E-mail: gaishili@hrbeu.edu.cn; yangpiaoping@hrbeu.edu.cn.

Notes

The authors declare no competing financial interest.

ACKNOWLEDGMENTS

We greatly acknowledge the financial support from the National Natural Science Foundation of China (NSFC 21271053, 21171045), Research Fund for the Doctoral Program of Higher Education of China (20112304110021), Program for New Century Excellent Talents in University, Harbin Sci.-Tech. Innovation Foundation (RC2012XK017012), and Fundamental Research Funds for the Central Universities of China.

REFERENCES

(1) Yang, P. P.; Gai, S. L.; Lin, J. *Chem. Soc. Rev.* **2012**, *41*, 3679−3698.
(2) Giri, S.; Trewyn, B. G.; Stellmaker, M. P.; Lin, V. S. Y. *Angew. Chem., Int. Ed.* **2005**, *44*, 5038−5044.
(3) Zhao, W. R.; Gu, J. L.; Zhang, L. X.; Chen, H. R.; Shi, J. L. *J. Am. Chem. Soc.* **2005**, *127*, 8916−8917.
(4) Torney, F.; Trewyn, B. G.; Lin, V. S. Y.; Wang, K. *Nat. Nanotechnol.* **2007**, *2*, 295−300.
(5) Muharnmad, F.; Guo, M.; Qi, W.; Sun, F.; Wang, A.; Guo, Y.; Zhu, G. *J. Am. Chem. Soc.* **2011**, *133*, 8778−8781.
(6) Liong, M.; Lu, J.; Kovochich, M.; Xia, T.; Ruehm, S. G.; Nel, A. E.; Tamanoi, F.; Zink, J. I. *ACS Nano* **2008**, *2*, 889−896.
(7) lrich, K. E.; Cannizzaro, S. M.; Langer, R. S.; Shakesheff, K. M. *Chem. Rev.* **1999**, *99*, 3181−3198.
(8) Nasongkla, N.; Shuai, X.; Ai, H.; Weinberg, B. D.; Pink, J.; Boothman, D. A.; Gao, J. *Angew. Chem., Int. Ed.* **2004**, *43*, 6323−6327.
(9) Bae, Y.; Fukushima, S.; Harada, A.; Kataoka, K. *Angew. Chem., Int. Ed.* **2003**, *42*, 4640−4643.
(10) Dalhaimer, P.; Engler, A. J.; Parthasarathy, R.; Discher, D. E. *Biomacromolecules* **2004**, *5*, 1714−1719.
(11) Wang, Y. J.; Bansal, V.; Zelikin, A. N.; Caruso, F. *Nano Lett.* **2008**, *8*, 741−745.
(12) Ha, C. S.; Gardella, J. A. *Chem. Rev.* **2005**, *105*, 4205−4232.
(13) Zhang, T. R.; Ge, J. P.; Hu, Y. X.; Zhang, Q.; Aloni, S.; Yin, Y. D. *Angew. Chem., Int. Ed.* **2008**, *47*, 5806−5811.
(14) Slowing, I. I.; Trewyn, B. G.; Giri, S.; Lin, V. S. Y. *Adv. Funct. Mater.* **2007**, *17*, 1225−1236.
(15) Kang, X. J.; Cheng, Z. Y.; Yang, D. M.; Ma, P. A.; Shang, M. M.; Peng, C.; Dai, Y. L.; Lin, J. *Adv. Funct. Mater.* **2013**, *22*, 1470−1481.
(16) Zhang, C. M.; Li, C. X.; Peng, C.; Chai, R. T.; Huang, S. S.; Yang, D. M.; Cheng, Z. Y.; Lin, J. *Chem.—Eur. J.* **2010**, *16*, 5672−5680.
(17) Kang, X. J.; Yang, D. M.; Dai, Y. L.; Shang, M. M.; Cheng, Z. Y.; Zhang, X.; Lian, H. Z.; Ma, P. A.; Lin, J. *Nanoscale* **2013**, *5*, 253−261.
(18) Yang, D. M.; Kang, X. J.; Ma, P. A.; Dai, Y. L.; Hou, Z. Y.; Cheng, Z. Y.; Li, C. X.; Lin, J. *Biomatrials* **2013**, *34*, 1601−1612.
(19) Chen, Y.; Chen, H. R.; Guo, L. M.; He, Q. J.; Chen, F.; Zhou, J.; Feng, J. W.; Shi, J. L. *ACS Nano* **2010**, *4*, 529−539.
(20) Caruso, F.; Caruso, R. A.; Mohwald, H. *Science* **1998**, *282*, 1111−1114.
(21) Dai, Y.; Ma, P. A.; Cheng, Z.; Kang, X.; Zhang, X.; Hou, Z.; Li, C.; Yang, D.; Zhai, X.; Lin, J. *ACS Nano* **2012**, *6*, 3327−3338.
(22) Zhu, Y. F.; Shi, J. L.; Shen, W. H.; Dong, X. P.; Feng, J. W.; Ruan, M. L.; Li, Y. S. *Angew. Chem., Int. Ed.* **2005**, *44*, 5083−5087.
(23) Bogershausen, A.; Pas, S. J.; Hill, J. A.; Koller, H. *Chem. Mater.* **2006**, *18*, 664−672.
(24) Dai, Y.; Zhang, C.; Cheng, Z.; Ma, P. A.; Li, C.; Kang, X.; Yang, D.; Lin, J. *Biomaterials* **2012**, *33*, 2583−2592.
(25) Zhao, D.; Feng, J.; Huo, Q.; Melosh, N.; Fredrickson, G. H.; Chmelka, B. F.; Stucky, G. D. *Science* **1998**, *279*, 548−552.
(26) Vallet-Regí, M.; Rámila, A.; del Real, R. P.; Pérez-Pariente, J. *Chem. Mater.* **2001**, *13*, 308−311.
(27) Muñoz, B.; Rámila, A.; Pérez- Pariente, J.; Díaz, I.; Vallet-Regí, M. *Chem. Mater.* **2003**, *15*, 500−503.
(28) Cheng, Y. L.; Brian, T. G.; Dusan, M. J.; Dsenija, J.; Shu, X.; Srdija, J.; Victor, S. Y. L. *J. Am. Chem. Soc.* **2003**, *125*, 4451−4459.
(29) Kresge, C. T.; Leonowicz, M. E.; Roth, W. J.; Vartuli, J. C.; Beck, J. S. *Nature* **1992**, *359*, 710−712.
(30) Qu, F. Y.; Zhu, G. S.; Huang, S. Y.; Li, S. G.; Sun, J. Y.; Zhang, D. L.; Qiu, S. L. *Microporous Mesoporous Mater.* **2006**, *92*, 1−9.
(31) Zhai, X. F.; Yu, M.; Cheng, Z. Y.; Hou, Z. Y.; Ma, P. A.; Yang, D. M.; Kang, X. J.; Dai, Y. L.; Wang, D.; Lin, J. *Dalton Trans.* **2011**, *40*, 12818−12825.
(32) Chen, Y.; Chen, H.; Zeng, D.; Tian, Y.; Chen, F.; Feng, J.; Shi, J. *ACS Nano* **2010**, *4*, 6001−6013.
(33) Deng, Y.; Qi, D.; Deng, C.; Zhang, X.; Zhao, D. *J. Am. Chem. Soc.* **2008**, *130*, 28−29.
(34) Jiao, F.; Jumas, J.-C.; Womes, M.; Chadwick, A. V.; Harrison, A.; Bruce, P. G. *J. Am. Chem. Soc.* **2006**, *128*, 12905−12909.
(35) Zhang, L.; Qiao, S.; Jin, Y.; Chen, Z.; Gu, H.; Lu, G. Q. *Adv. Mater.* **2008**, *20*, 805−809.
(36) Zhao, W.; Chen, H.; Li, Y.; Li, L.; Lang, M.; Shi, J. *Adv. Funct. Mater.* **2008**, *18*, 2780−2788.
(37) Zhu, Y.; Ikoma, T.; Hanagata, N.; Kaskel, S. *Small* **2010**, *6*, 471−478.
(38) Sinha, A. K.; Seelan, S.; Tsubota, S.; Haruta, M. *Angew. Chem., Int. Ed.* **2004**, *43*, 1546−1548.
(39) Lee, J.; Park, J. C.; Song, H. *Adv. Mater.* **2008**, *20*, 1523−1528.
(40) Botella, P.; Corma, A.; Navarro, M. T. *Chem. Mater.* **2007**, *19*, 1979−1983.
(41) Fukuoka, A.; Araki, H.; Kimura, J.; Sakamoto, Y.; Higuchi, T.; Sugimoto, N.; Inagaki, S.; Ichikawa, M. *J. Mater. Chem.* **2004**, *14*, 752−756.
(42) Kim, J. Y.; Yoon, S. B.; Yu, J.-S. *Chem. Commun.* **2003**, 790−791.
(43) Xu, Z.; Li, C.; Kang, X.; Yang, D.; Yang, P.; Hou, Z.; Lin, J. *J. Phys. Chem. C* **2010**, *114*, 16343−16350.
(44) Guerrero-Martinez, A.; Perez-Juste, J.; Liz-Marzan, L. M. *Adv. Mater.* **2010**, *22*, 1182−1195.
(45) Kim, J.; Kim, H. S.; Lee, N.; Kim, T.; Kim, H.; Yu, T.; Song, I. C.; Moon, W. K.; Hyeon, T. *Angew. Chem., Int. Ed.* **2008**, *47*, 8438−8441.
(46) Kim, J.; Lee, J. E.; Lee, J.; Yu, J. H.; Kim, B. C.; An, K.; Hwang, Y.; Shin, C. H.; Park, J. G.; Hyeon, T. *J. Am. Chem. Soc.* **2006**, *128*, 688−689.
(47) Klajn, R.; Stoddart, J. F.; Grzybowski, B. A. *Chem. Soc. Rev.* **2010**, *39*, 2203−2237.
(48) Liong, M.; Lu, J.; Kovochich, M.; Xia, T.; Ruehm, S. G.; Nel, A. E.; Tamanoi, F.; Zink, J. I. *ACS Nano* **2008**, *2*, 889−896.
(49) Rosenholm, J. M.; Peuhu, E.; Eriksson, J. E.; Sahlgren, C.; Linden, M. *Nano Lett.* **2009**, *9*, 3308−3311.
(50) Liong, J. M.; Li, Z. X.; Zink, J. I.; Tamanoi, F. *Small* **2010**, *6*, 1794−1805.
(51) Morelli, C.; Maris, P.; Sisci, D.; Perrotta, E.; Brunelli, E.; Perrotta, I.; Panno, M. L.; Tagarelli, A.; Versace, C.; Casula, M. F.; Testa, F.; Ando, S.; Nagy, J. B.; Pasqua, L. *Nanoscale* **2011**, *3*, 3198−3207.
(52) He, Q.; Zhang, J.; Shi, J.; Zhu, Z.; Zhang, L.; Bu, W.; Guo, L.; Chen, Y. *Biomaterials* **2010**, *31*, 1085−1092.

(53) Sertchook, H.; Elimelech, H.; Makarov, C.; Khalfin, R.; Cohen, Y.; Shuster, M.; Babonneau, F.; Avnir, D. *J. Am. Chem. Soc.* **2007**, *129*, 98−108.
(54) Vivero-Escoto, J. L.; Taylor- Pashow, K. M. L.; Huxford, R. C.; Della Rocca, J.; Okoruwa, C.; An, H.; Lin, W.; Lin, W. *Small* **2011**, *7*, 3519−3528.
(55) Yang, Q.; Ma, S.; Li, J.; Xiao, F.; Xiong, H. *Chem. Commun.* **2006**, 2495−2497.
(56) Schrum, K. F.; Lancaster, J. M.; Johnston, S. E.; Gilman, S. D. *Anal. Chem.* **2000**, *72*, 4317−4321.
(57) Brokmann, X.; Hermier, J. P.; Messin, G.; Desbiolles, P.; Bouchaud, J. P.; Dahan, M. *Phys. Rev. Lett.* **2003**, *90*, 120601−1.
(58) Hohng, S.; Ha, T. J. *Am. Chem. Soc.* **2004**, *126*, 1324−1325.
(59) Fischer, H. C.; Liu, L. C.; Pang, K. S.; Chan, W. C. W. *Adv. Funct. Mater.* **2006**, *16*, 1299−1305.
(60) Blasse, G.; Grabmaier, B. C. *Luminescent Materials*; Springer: Berlin, 1994; Ch. 4.
(61) Liu, Y.; Tu, D.; Zhu, H.; Li, R.; Luo, W.; Chen, X. *Adv. Mater.* **2010**, *22*, 3266−3271.
(62) Yeh, C.-W.; Chen, W.-T.; Liu, R.-S.; Hu, S.-F.; Sheu, H.-S.; Chen, J.-M.; Hintzen, H. T. *J. Am. Chem. Soc.* **2012**, *134*, 14108−14117.
(63) Hao, J.; Zhang, Y.; Wei, X. *Angew. Chem., Int. Ed.* **2011**, *50*, 6876−6880.
(64) Tu, D.; Liu, L.; Ju, Q.; Liu, Y.; Zhu, H.; Li, R.; Chen, X. *Angew. Chem., Int. Ed.* **2011**, *50*, 6306−6310.
(65) Chen, W.-T.; Sheu, H.-S.; Liu, R.-S.; Attfield, J. P. *J. Am. Chem. Soc.* **2012**, *134*, 8022−8025.
(66) Zhang, T.; Zhu, X.; Cheng, C. C. W.; Kwok, W.-M.; Tam, H.-L.; Hao, J.; Kwong, D. W. J.; Wong, W.-K.; Wong, K.-L. *J. Am. Chem. Soc.* **2011**, *133*, 20120−20122.
(67) Liu, T.-C.; Kominami, H.; Greer, H. F.; Zhou, W.; Nakanishi, Y.; Liu, R.-S. *Chem. Mater.* **2012**, *24*, 3486−3492.
(68) Gai, S.; Yang, P.; Li, C.; Wang, W.; Dai, Y.; Niu, N.; Lin, J. *Adv. Funct. Mater.* **2010**, *20*, 1166−1172.
(69) Yang, P.; Quan, Z.; Hou, Z.; Li, C.; Kang, X.; Cheng, Z.; Lin, J. *Biomaterials* **2009**, *30*, 4786−4795.
(70) Lin, Y.-S.; Haynes, C. L. *Chem. Mater.* **2009**, *21*, 3979−3986.
(71) Hao, L. Y.; Zhu, C. L.; Jiang, W. Q.; Chen, C. N.; Hu, Y.; Chen, Z. Y. *J. Mater. Chem.* **2004**, *14*, 2929−2934.
(72) Yang, J.; Lee, J.; Kang, J.; Lee, K.; Suh, J.-S.; Yoon, H.-G.; Huh, Y.-M.; Haam, S. *Langmuir* **2008**, *24*, 3417−3421.
(73) Zhu, Y.; Ikoma, T.; Hanagata, N.; Kaskel, S. *Small* **2010**, *6*, 471−478.
(74) Wu, H.; Zhang, S.; Zhang, J.; Liu, G.; Shi, J.; Zhang, L.; Cui, X.; Ruan, M.; He, Q.; Bu, W. *Adv. Funct. Mater.* **2011**, *21*, 1850−1862.
(75) Zhang, L.; Wang, T.; Yang, L.; Liu, C.; Wang, C.; Liu, H.; Wang, Y. A.; Su, Z. *Chem.—Eur. J.* **2012**, *18*, 12512−12521.
(76) Lou, L.; Boyer, D.; Chadeyron, G.; Bernstein, E.; Mahiou, R.; Mugnier, J. *Opt. Mater.* **2000**, *15*, 1−6.
(77) Bertrand-Chadeyron, G.; Mahiou, R.; El-Ghozzi, M.; Arbus, A.; Zambon, D.; Cousseins, J. C. *J. Lumin.* **1997**, *72*−*74*, 564−566.
(78) Boyer, D.; Bertrand, G.; Mahiou, R. *J. Lumin.* **2003**, *104*, 229−237.
(79) Li, Y.; Zhang, J.; Zhang, X.; Luo, Y.; Lu, S.; Ren, X.; Wang, X.; Sun, L.; Yan, C. *Chem. Mater.* **2009**, *21*, 468−475.
(80) Song, H.; Yu, H.; Pan, G.; Bai, X.; Dong, B.; Zhang, X. T.; Hark, S. K. *Chem. Mater.* **2008**, *20*, 4762−4767.
(81) Lin, C.; Kong, D.; Liu, X.; Wang, H.; Yu, M.; Lin, J. *Inorg. Chem.* **2007**, *46*, 2674−2681.
(82) Li, Z. H.; Zeng, J. H.; Li, Y. D. *Small* **2007**, *3*, 438−443.
(83) Hou, Z. Y.; Li, C. X.; Ma, P. A.; Cheng, Z. Y.; Li, X. J.; Zhang, X.; Dai, Y. L.; Yang, D. M.; Lian, H. Z.; Lin, J. *Adv. Funct. Mater.* **2012**, *22*, 2713−2722.
(84) Xu, Z. H.; Ma, P. A.; Li, C. X.; Hou, Z. Y.; Zhai, X. F.; Huang, S. S.; Lin, J. *Biomaterials* **2011**, *32*, 4161−4173.
(85) Wang, L.; Li, Y. *Nano Lett.* **2006**, *6*, 1645−1649.
(86) Song, Y.; You, H.; Huang, Y.; Yang, M.; Zheng, Y.; Zhang, L.; Guo, N. *Inorg. Chem.* **2010**, *49*, 11499−11504.
(87) Wang, Z.-L.; Hao, J.; Chan, H. L. W. *J. Electrochem. Soc.* **2010**, *157*, J315−J318.
(88) Fan, W.-Q.; Feng, J.; Song, S.-Y.; Lei, Y.-Q.; Zheng, G.-L.; Zhang, H.-J. *Chem.—Eur. J.* **2010**, *16*, 1903−1910.
(89) Wang, G.; Qin, W.; Zhang, D.; Wang, L.; Wei, G.; Zhu, P.; Kim, R. *J. Phys. Chem. C* **2008**, *112*, 17042−17045.
(90) Li, Y.-J.; Yan, B. *Inorg. Chem.* **2009**, *48*, 8276−8285.
(91) Lu, H.-F.; Yan, B.; Liu, J.-L. *Inorg. Chem.* **2009**, *48*, 3966−3975.
(92) Yu, M.; Lin, J.; Fang, J. Y. *Chem. Mater.* **2005**, *17*, 1783−1791.